PAPER

# Analysis of MRI Slotted Tube Resonator Having a Shield of Conducting Circular Cylinder

Qiang CHEN†, Kunio SAWAYA†, Saburo ADACHI†, Hisaaki OCHI††
*and* Etsuji YAMAMOTO††, *Members*

**SUMMARY** A slotted tube resonator (STR) having a shield of conducting circular cylinder which is used as a probe for the magnetic resonance imaging (MRI) is analyzed by using the variational method and the dyadic Green's function of a circular waveguide. Three surface current modes are employed to expand the currents on the STR. Quadruple integrals appearing in the variational expression are evaluated analytically for saving the CPU time. Resonant frequency, $Q$ value and the magnitude of magnetic field distributions for various radii of the shields are obtained to show the effects of the shield. Some measured date are compared with the theoretical results to confirm the validity of the present analysis.

***key words:*** *MRI, NMR, slotted tube resonator, shield, antenna, probe*

## 1. Introduction

MRI (Magnetic Resonance Imaging) system, which can show us high-quality cross-sectional images in an arbitrary direction of a human body, has been recognized as a new powerful technique for medical diagnosis and has gradually come to be employed in recent years. At the same time, many researches and investigations have been carried out to improve the performance of the MRI system.

In the MRI system, an RF probe is used to emit a uniform RF magnetic field over the human body and receive the response signals from the body. Several kinds of the RF probes have been developed. Slotted tube resonator (STR) is one kind of them which was proposed by Alderman and Grant.[1] Since the STR is composed of complicated conducting strips, the theoretical analysis is difficult. Although approximate numerical analysis of the STR such as a method using cylindrical-window model and the finite element method has been made,[2] these solutions are only for a two-dimensional model. Therefore a numerical analysis of a more realistic model of the STR has been required for a practical use.

Recently, the STR in free space has been studied by the present authors[3] and some numerical solutions such as the current distribution, the electromagnetic field distribution and the input impedance were obtained by a wire-grid approximation. This work has clarified how the STR is resonated and how it can produce a uniform magnetic field. However, the STR is commonly used inside a shield of a conducting cylinder to eliminate external noise coming from other equipments such as a gradient magnetic field coil and a superconducting magnet around the STR. Since a large shield requires a large surrounding coil and a large magnet, and increases the cost of the production, the radius of the shield is desired to be as small as possible. On the other hand, a small shield exerts some effects on the properties of the STR. Therefore, it is very important to analyze the STR placed inside a conducting circular cylinder to clarify the effects of the cylindrical shield on the properties of the STR, quantitatively.

In this paper, the STR having a shield of circular cylinder is analyzed by using the dyadic Green's function of a circular waveguide and the variational method, where the circular cylinder is assumed to be perfectly conducting and infinitely long. A method using three surface current modes is proposed to expand the surface current on the STR for the variational analysis. Numerical results such as the resonant frequency, the sensitivity and $Q$ value of the STR having the shield of various diameters are presented to show the effects of the circular shield. The theoretical solutions are compared with the results of experiment to confirm the validity of the analysis. Distribution of the magnetic field emitted by the STR is also illustrated. Although a human body is located inside the STR in the practical use and it also exerts effects on the properties of the STR, the human body is not included in the present analysis since our interest is focused on the effects of the shield.

## 2. Formulation

Figure 1 shows the configuration of the STR having a conducting circular cylindrical shield. The STR is composed of six parts, i.e., two vertical strips called arms, two outer rings with radius $R_a$ called wings which have four cuts as shown in the figure, and

Manuscript received June 10, 1992.
Manuscript revised November 17, 1992.

† The authors are with the Faculty of Engineering, Tohoku University, Sendai-shi, 980 Japan.
†† The authors are with the Central Research Laboratory, Hitachi, Ltd., Kokubunji-shi, 185 Japan.

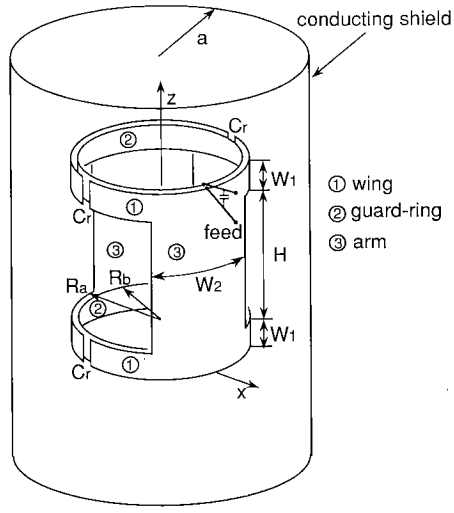


Fig. 1 Geometry of slotted tube resonator having shield of conducting circular cylinder.

two inner rings with radius $R_b$ called guard-rings. Teflon sheets are inserted between the guard-rings and the wings. The four cuts on the wings are bridged by four chip capacitors $C_r$ for tuning the resonant frequency and a capacitor $C_m$ is connected parallel to the feed point for the impedance matching. The cylinder with radius $a$ is located coaxially with the STR and is assumed to be infinitely long for the analysis.

The equivalent circuit method has been used to analyze the STR.[4] However, the accuracy of the method is not satisfactory since the definition of the $L$, $C$ and $R$ becomes indefinable as the RF frequency used in MRI becomes higher and higher (64 MHz system is under research now). The moment method analysis using a subdomain expansion technique can be used to obtain more accurate solution than the equivalent circuit method, but it requires a large number of segments for the structure composed of curved-planar strips and a great amount of CPU time for computation. Therefore, we adopt the variational method to analyze the characteristics of the STR. It is very important to choose a set of suitable expansion functions in order to expand the surface current in the variational method. Fortunately, the current distribution of the STR in free space has been obtained previously.[3] Referring to the current distribution in free space, we propose a method using three kinds of expansion modes for the surface current as shown in Fig. 2. The modes are defined by vector functions as

$$\begin{cases} |f_1| = 2 & \text{mode 1} \\ |f_2| = \cos 0.5\varphi & \text{mode 2} \\ |f_3| = |\sin \varphi| & \text{mode 3} \end{cases} \tag{1}$$

where the directions of each vector are shown by arrows in Fig. 2. The mode 1 is used to express the current of the outer structure of the STR. In the

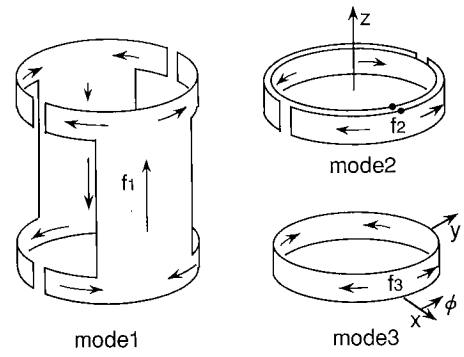


Fig. 2 Three expansion modes of surface current on slotted tube resonator.

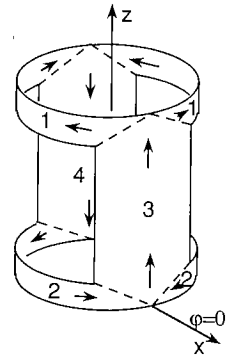


Fig. 3 Four submodes of the mode 1.

previous analysis,[3] we have found the current on the STR is almost uniform and the flow of the current can be regarded as a uniform current loop. The loop current is especially strong at the resonant frequency and dominantly contributes to produce the homogeneous magnetic field in the interior region. Although the STR is shielded by the conducting cylinder in the present case, the uniform current distribution is not considered to change significantly. Mode 1 is a balanced current mode and is expected to express the dominant loop current observed in the free space analysis. Mode 2 is used to express the current on the upper guard-ring, the upper wing and feeding conductor. The purpose of the use of the mode 3 is to expand the current on the lower guard ring which is isolated from the other conductors. Each of the three modes is assumed to be uniformly distributed along the transverse direction to the current flow.

The three modes are selected not only to conform with the current distribution in the case of free space, but also to be strictly continuous. If there is any discontinuity in the current distribution, a charge will appear there, which is unreasonable from the physical point of view and leads to a divergence of the double infinite series appearing in the dyadic Green's function. The mode 1 current has the $z$-directed current and the $\varphi$-directed current, and the connection between these two directed currents should be carefully determined,

although the mode 1 is a constant current distribution. Figure 3 shows the connection employed in this paper to obtain the continuity between the currents of the different directions. The mode 1 is further divided into four submodes and each submode has only $z$-directed or $\varphi$-directed current. The self impedance of the mode 1 $Z_{11}$ is calculated by a summation of the impedance between these submodes as shown in appendix. Although the calculation of the self and mutual impedance of the submodes does not converge because of the discontinuity of the current of each submode, the calculation of the total $Z_{11}$ gives a good convergence. The current of the mode 2 flowing toward the $\pm\varphi$ direction has similar discontinuity at $\varphi=\pi$ unless the mode function is set to be zero at $\varphi=\pi$. The mode 2 current should have a maximum value at $\varphi=0$, where the driving current is fed. By the same reason, the function of the mode 3 should be zero at $\varphi=0$ and $\varphi=\pi$. Taking account of the reasons described above and the fact that the formulation is easy, sinusoidal functions $\cos(\varphi/2)$ and $|\sin\varphi|$ are used as the mode 2 and mode 3 functions, respectively.

Since the dimensions of the STR are electrically small at the operating frequency (about 21 MHz), the three modes mentioned above are enough for the variational analysis.

As a first step of the variational approach, the current distribution $\boldsymbol{I}(\boldsymbol{R})$ on the surface of th STR is expanded by the three kinds of current modes described above, i.e.,

$$\boldsymbol{I}(\boldsymbol{R})=\sum_{k=1}^{3}\alpha_k \boldsymbol{f}_k(\boldsymbol{R}) \tag{2}$$

where $\alpha_k$ are unknown coefficients. The variational expression for the input impedance can be expressed by

$$Z_{in}=\frac{1}{4\alpha_2^2}\Big[j\omega\mu\int_S\int_{S'}\boldsymbol{I}(\boldsymbol{R})\cdot\bar{\boldsymbol{G}}(\boldsymbol{R},\boldsymbol{R}')\cdot\boldsymbol{I}(\boldsymbol{R}')\,dS'dS+2\Big(\alpha_1-\cos\Big(\frac{\pi}{4}\Big)\alpha_2\Big)^2 Z_c+2\alpha_1^2 Z_c\Big] \tag{3}$$

where $Z_c=1/j\omega C_c$, and $C_r$ is the chip capacitor shown in Fig. 1. $\bar{\boldsymbol{G}}(\boldsymbol{R},\boldsymbol{R}')$ denotes the dyadic Green's function of a circular cylindrical waveguide.[5] According to the variational theory, the partial differential of $Z_{in}$ with respect to each coefficient $\alpha_k$ should be zero. Assuming $\alpha_2$ to be unity, the following equations can be obtained.

$$\begin{cases}\dfrac{\partial Z_{in}}{\partial\alpha_1}=0\\ \alpha_2=1\\ \dfrac{\partial Z_{in}}{\partial\alpha_3}=0\end{cases} \tag{4}$$

Substituting (3) into (4), we get a simultaneous equation given by

$$\begin{cases}(Z_{11}+4Z_c)\alpha_1+Z_{13}\alpha_3=-Z_{12}+\sqrt{2}\,Z_c\\ Z_{13}\alpha_1+Z_{33}\alpha_3=-Z_{32}\end{cases} \tag{5}$$

where $Z_{ij}$ denotes the self and the mutual impedance between the three modes, and is defined as

$$Z_{ij}=j\omega\mu\int_S\int_{S'}\boldsymbol{f}_i(\boldsymbol{R})\cdot\bar{\boldsymbol{G}}(\boldsymbol{R},\boldsymbol{R}')\cdot\boldsymbol{f}_j(\boldsymbol{R}')\,dS'dS \tag{6}$$

If we solve Eq. (5), we can obtain the values of coefficients $\alpha_k$, $k=1\sim3$ and get the current distribution. The input impedance can be obtained by Eqs. (3) and (5), and it is expressed simply as

$$Z_{in}=\frac{1}{4}[\alpha_1 Z_{12}+Z_{22}+\alpha_3 Z_{32}+(1-\sqrt{2}\,\alpha_1)Z_c] \tag{7}$$

In all the steps described above, the most important and difficult work is the calculation of the self and mutual impedance $Z_{ij}$ in Eq. (6) since it involves a quadruple integral over the surface of the STR and a double summation of infinite series which are related to the eigenfunction expansion appearing in the dyadic Green's function. Numerical calculation of the quadruple integral and the double summation requires a large amonut of CPU time. Therefore, we evaluate the quadruple integral analytically and obtain $Z_{ij}$ in the form of only the double summation. The analytical integration process is lengthy and the expressions of $Z_{ij}$ are very complicated.[6] Therefore, we show the procedure and the resultant expression of only $Z_{11}$ as an example in appendix.

## 3. Results

As a numerical example, the characteristics of a STR used for a human head is discussed. The radius of wing is $R_a=128$ mm and the radius of the guard-ring is $R_b=126$ mm. The height of the slots is $H=230$ mm and the aperture angle of that is 93° which corresponds to the width of the arms, $W_2=195$ mm. The width of the wing and the guard-ring is $W_1=35$ mm. The capacitance $C_r$ and $C_m$ are 205 pF and 164 pF, respectively. The copper loss of the STR and the loss of the tantalum capacitors $C_r$ and $C_m$ (Q factor$=10^3$) are incorporated in the calculation, whereas the copper loss of the shield is neglected. The effect of the Teflon sheets between the guard-rings and the wings is also neglected.

In order to show the validity of the theoretical analysis, we carried out an experiment in which the input impedance of the STR inside a cylinder was measured. The STR is fabricated with copper strips having a thickness of about 0.5 mm. The configuration of the STR used in the experiment is the same as that of the theoretical model. Three kinds of circular

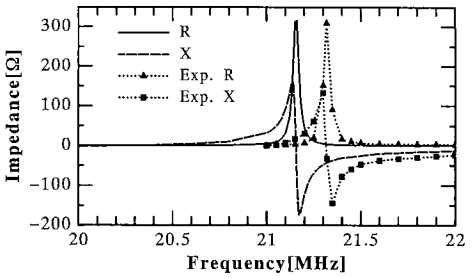


Fig. 4 Input impedance of slotted tube resonator as a function of frequency for $a/R_a=2.19$.

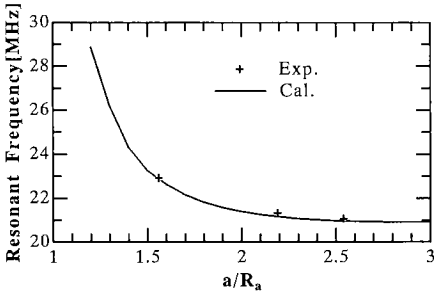


Fig. 5 Resonant frequency vs. the radius of the circular shield.

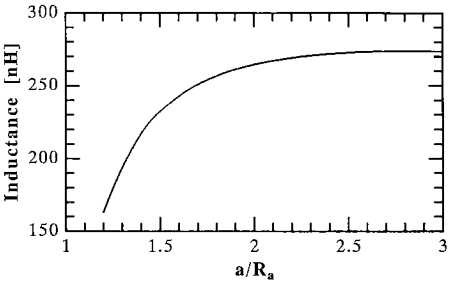


Fig. 6 The equivalent inductance $L$ vs. the radius of the shield.

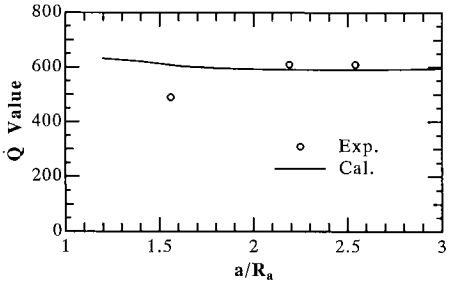


Fig. 7 Value of $Q$ vs. the radius of the shield.

copper cylinders were used in the experiment as the shield. They are all about 1.5 m long and have radius of 200 mm, 280 mm and 325 mm, respectively.

The behavior of the input impedance with ratio of $a/R_a=2.19$ is shown in Fig. 4. Experimental results are also plotted in the same figure. Although a slight difference of the resonant frequency of about 160 kHz is observed, the agreement between the theory and the experiment is satisfactory.

Since the STR is used at the resonant frequency which has to be tuned to the spin frequency of an atomic nucleus to be imaged, it is important to know the shift of the resonant frequency when the radius of the cylinder is changed. The shift of the resonant frequency as a function of the radius of the cylinder is shown in Fig. 5. Good agreement between the theory and the experiment is again obtained. It is noted that the cylinder with the radius $a \leqq 2R_a$ will increase the resonant frequency of the STR significantly.

The equivalent inductance $L$ of the STR[4] can be obtained approximately by calculating $L = \mathrm{Re}\,[Z_{11}/4j\omega]$ because the mode 1 seems to be an inductance coil having 2 unit currents and the magnetic field emitted by the mode 1 is almost the same as that by the entire STR. Figure 6 shows the shift to the $L$ as a function of radius of the shield. It is noted that the inductance decreases as the radius of the shield decreases and as the result the resonant frequency increases.

Since the frequency is within a cut-off range of the circular waveguide and no lossy dielectric body is located inside the STR, the power loss is due to the copper loss of the conductors of the STR and the shield and the dielectric loss of the capacitors. In the present analysis, the copper loss of the STR and the dielectric loss of the capacitors are taken into account but the loss of the shield is neglected. If the copper loss is dominant, the values of the $Q$ decreases as the radius of the shield decreases. On the other hand, the $Q$ value is almost independent of the value of $a/R_a$ in the case that the dielectric loss is dominant. These can be explained by discussing an equivalent $L$-$C$ resonant circuit. An equivalent resistance $R$ in the resonant circuit, which is connected to the equivalent inductance $L$ in series and represents the copper loss of antenna conductor, is proportional to the square root of the frequency. It is easily found that the value of the $Q$ due to the equivalent resistance $R$ is proportional to $L^{3/4}$. On the other hand, An equivalent conductance $G$ connected to the equivalent capacitor $C$ in parallel is proportional to $\omega C$ provided that the loss tangent of the dielectric material is constant. Therefore, the $Q$ due to the dielectric loss of the capacitor $C$ is independent of the value of $L$. Since the power loss due to the dielectric loss is several times greater than that of the copper loss in the present numerical example, the $Q$ is almost independent of the equivalent inductance $L$. Therefore, the theoretical results in Fig. 7 show that the $Q$ value almost remains constant when the $a/R_a$ decreases even though the $L$ decreases as shown in Fig. 6.

Experimental results of the $Q$ is also plotted in Fig. 7. Theoretical results and the measured data agree

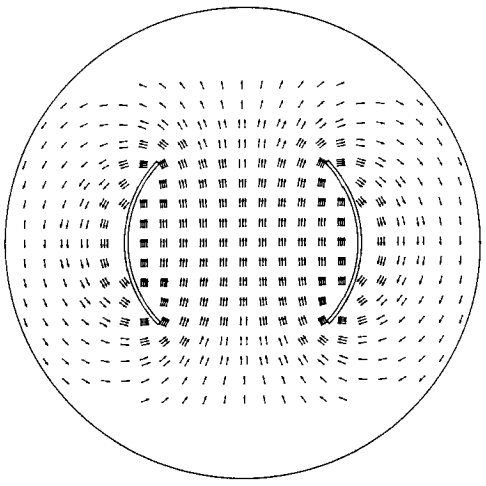

(a)

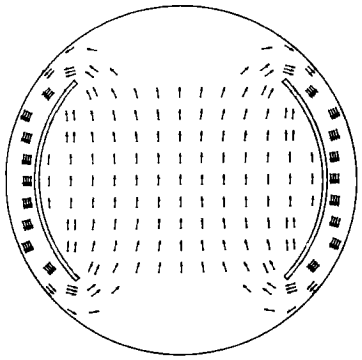

(b)

| arrows | $H[A/m]$ |
|---|---|
| | $0 \sim 3$ |
| ↑ | $3 \sim 6$ |
| ⇑ | $6 \sim 9$ |
| ⇈ | $9 \sim 12$ |
| ⇈ | $12 \sim \infty$ |

Fig. 8 Distribution of magnitude of magnetic field for (a) $a/R_a=2$ and (b) $a/R_a=1.2$.

well except for small $a/R_a$. When the shield is too close to the STR, the measured $Q$ is smaller than the theoretical $Q$. This phenomenon may be caused by an increase of the copper loss of the STR as well as the conducting wall of the shielding cylinder. The copper loss of the shield is neglected in the present analysis, but it increases significantly as the radius of the shield decreases.[2] Therefore, the discrepancy between the theory and the experiment for the case of a small $a/R_a$ may be caused by the neglect of the loss of the shield.

Figure 8 shows the mapping of magnitudes of the magnetic field distribution on the cross section of the

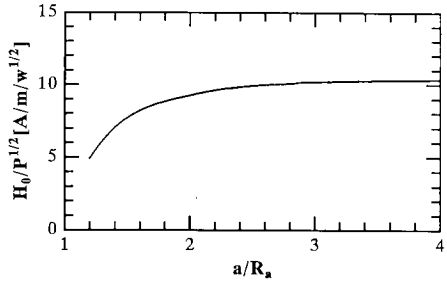


Fig. 9 The ratio $H_0/\sqrt{P}$ as a function of $a/R_a$.

STR at height of $z=W_1+H/2$ for ratio of $a/R_a=1.2$ and 2 where the input power is 1 watt.

The arrow indicates the direction of the magnetic field. Since the variational expression of the input impedance has a stationary property, the input impedance can be obtained accurately. However, the boundary condition is not satisfied completely and the field in the close vicinity of the antenna conductor can not be obtained accurately. Therefore, the magnetic field in the close vicinity of the antenna conductor is not shown in Fig. 8. The larger shielding cylinder brings little effects on the field distribution, and a uniform field distribution similar to that for the case of free space is observed.[3] While, the smaller shielding cylinder tends to disturb the field and makes the magnitude weak in the imaging area significantly.

The ratio $H_0/\sqrt{P}$, which predicts the sensitivity of the MRI probe, is shown in Fig. 9 as a function of the ratio $a/R_a$, where $H_0$ is the magnitude of the magnetic field at the center of the STR and $P$ denotes the total input power. The ratio of $a/R_a$ is required to be greater than about 2 in order to obtain a high sensitivity of the STR as shown in Fig. 9.

## 4. Conclusion

Slotted tube resonator (STR) having a conducting circular cylinder has been analyzed by using of the variational method and the dyadic Green's function of a circular waveguide. A method using three surface current modes has been proposed to expand surface current on the STR. Because of the presence of the cylindrical shield, the resonant frequency increases rapidly and the sensitivity of the STR decreases greatly when the ratio of $a/R_a$ becomes less than about 2. The present analysis has been confirmed to be valid by comparing with the experiment. Although the resonator has a complicated strip structure, the analysis costs little CPU time and accuracy of the results is satisfactory. The numerical results obtained by the present method are very helpful for the design of the STR having the shield. The STR should be analyzed further when a lossy dielectric body is located to clarify the effects of the body.

## References


(1) Alderman, D. W. and Grant, D. M., "An Efficient Decoupler Coil Design Which Reduces Heating in Conductive Samples in Superconducting Spectrometers," *J. Magn. Reson.*, vol. 36, no. 3, pp. 447–451, Dec. 1979.

(2) Kost, G. J., Anderson, S. E., Matson, G. B. and Conboy, C. B., "A Cylindrical-Window NMR Probe with Extended Tuning Range for Studies of the Developing Heart," *J. Magn. Reson.*, vol. 82, pp. 238–252, 1989.

(3) Chen, Q., Sawaya, K., Adachi, S., Ochi, H. and Yamamoto, E., "Analysis of Slotted Tube Resonator for MRI," *IEICE Trans., Commun.*, vol. E75-B-II, no. 8, pp. 602–605, Aug. 1992.

(4) Hong, D. H., Lee, S. W., Ra, J. W. and Cho, Z. H., "Whole Body Slotted Tube Resonator (STR) for Proton NMR Imaging at 2.0 Tesla," *Magnetic Resonant Imaging*, vol. 5, no. 3, pp. 239–243, 1987.

(5) Tai, C. T., *Dyadic Green's Functions in Electromagnetic Theory*, Intext Educational Publishers, 1971.

(6) Chen, Q., Sawaya, K., Adachi, S., Ochi, H. and Yamamoto, E., "MRI Slotted Tube Resonator in Circular Conducting Cylinder," *Technical Report of IEICE*, A. P92-101, pp. 9–16, Dec. 1992.


## Appendix

In this appendix, the results of the modification of the quadruple integrals into a form not involving any integral are presented for the case of $Z_{11}$. As illustrated in Fig. 3, the mode 1 is further expanded into four submodes. The impedance between the four submodes can be obtained by

$$S_{ij}=j\omega\mu\int_{s_j}\int_{s_i}\boldsymbol{f}_1(\boldsymbol{R})\cdot\bar{\boldsymbol{G}}(\boldsymbol{R},\boldsymbol{R}')\cdot\boldsymbol{f}_1(\boldsymbol{R}')\,ds_i'ds_j \tag{A·1}$$

where $S_{ij}$ is the impedance between the submode $i$ and submode $j$. Substituting $\boldsymbol{f}_1(\boldsymbol{R})$ expressed in Eq. (1) and the dyadic Green's function of a circular waveguide $\bar{\boldsymbol{G}}(\boldsymbol{R},\boldsymbol{R}')$[5] into Eq. (A·1), we obtain

$$\begin{aligned}S_{11}=&j\omega\mu\frac{4R_a^2}{W_1^2}\int_0^{W_1}dz\int_0^{W_1}dz'\int_{-\frac{z}{\alpha}+\frac{\theta_0}{2}}^{\pi+\frac{z'}{\alpha}-\frac{\theta_0}{2}}d\varphi\\&\cdot\int_{-\frac{z'}{\alpha}+\frac{\theta_0}{2}}^{\pi+\frac{z'}{\alpha}-\frac{\theta_0}{2}}d\varphi' G_{\varphi\varphi}(R_a,\varphi,z,R_a,\varphi',z')\\=&\frac{\omega\mu R_a^2}{4\pi W_1^2}\sum_{n=0}^{\infty}\sum_{m=1}^{\infty}(2-\delta_0)\left[\frac{J_n^2(\mu R_a)}{I_\mu k_\mu}I_{11}(k_\mu)\right.\\&\left.+\frac{k_\lambda n^2J_n^2(\lambda R_a)}{\lambda^2I_\lambda k^2R_a^2}I_{11}(k_\lambda)\right]\end{aligned} \tag{A·2}$$

$$\begin{aligned}I_{11}(\xi)=&\frac{(1-(-1)^n)^2}{n^2}\frac{4d^2}{1-\xi^2d^2}\left[j\xi\left(\frac{d}{2}\sin 2\gamma\right.\right.\\&\left.+W_1\right)+\frac{\Lambda^+(\gamma)\Lambda^-(\gamma)+d^2\xi^2}{1-d^2\xi^2}\\&\left.-\frac{2jd\xi\Lambda(\gamma)e^{-j\xi W_1}}{1-d^2\xi^2}\right]\end{aligned} \tag{A·3}$$

$$\begin{aligned}S_{12}=&j\omega\mu\frac{4R_a^2}{W_1^2}\int_{H+W_1}^{H+2W_1}dz\int_0^{W_1}dz'\int_{-\frac{z-H-W_1}{\alpha}+\frac{\theta_0}{2}}^{\pi+\frac{z-H-W_1}{\alpha}-\frac{\theta_0}{2}}d\varphi\\&\cdot\int_{\frac{z'}{\alpha}}^{\pi-\frac{z'}{\alpha}}d\varphi' G_{\varphi\varphi}(R_a,\varphi,z,R_a,\varphi',z')\\=&\frac{\omega\mu R_a^2}{4\pi W_1^2}\sum_{n=0}^{\infty}\sum_{m=1}^{\infty}(2-\delta_0)\left[\frac{J_n^2(\mu R_a)}{I_\mu k_\mu}I_{12}(k_\mu)\right.\\&\left.+\frac{k_\lambda n^2J_n^2(\lambda R_a)}{\lambda^2I_\lambda k^2R_a^2}I_{12}(k_\lambda)\right]\end{aligned} \tag{A·4}$$

$$\begin{aligned}I_{12}(\xi)=&\frac{(1-(-1)^n)^2}{n^2}\frac{4d^2}{(1-\xi^2d^2)^2}[\Lambda^{-2}(\gamma)e^{-j\xi H}\\&-2jd\xi\Lambda^-(\gamma)e^{-j\xi(H+W_1)}\\&-d^2\xi^2e^{-j\xi(H+2W_1)}]\end{aligned} \tag{A·5}$$

$$\begin{aligned}S_{13}=&-j\omega\mu\frac{8R_a^2}{W_1W_2}\int_0^{W_1}dz\int_{\frac{z}{\alpha}}^{\pi-\frac{z}{\alpha}}d\varphi\int_0^{\frac{\theta_0}{2}}d\varphi'\\&\cdot\int_{\alpha\varphi'}^{-\alpha\varphi'+H+2W_1}dz' G_{z\varphi}(R_a,\varphi,z,R_a,\varphi',z')\\=&\frac{\omega\mu R_a^2}{4\pi W_1W_2}\sum_{n=0}^{\infty}\sum_{m=1}^{\infty}(2-\delta_0)\frac{jnJ_n^2(\lambda R_a)}{I_\lambda k^2R_a}I_{13}(k_\lambda)\end{aligned} \tag{A·6}$$

$$\begin{aligned}I_{13}(\xi)=&\frac{1-(-1)^n}{n^2}\frac{8d}{j\xi(1-d^2\xi^2)}\left[j\xi\left(\frac{d}{2}\sin 2\gamma\right.\right.\\&\left.+W_1\right)+\frac{\Lambda^+(\gamma)\Lambda^-(\gamma)+d^2\xi^2}{1-d^2\xi^2}\\&-\frac{1}{1-d^2\xi^2}(2jd\xi\Lambda^+(\gamma)e^{-j\xi W_1}\\&+\Lambda^{-2}(\gamma)e^{-j\xi H}-2jd\xi\Lambda^-(\gamma)e^{-j\xi(H+W_1)}\\&\left.-d^2\xi^2e^{-j\xi(H+2W_1)})\right]\end{aligned} \tag{A·7}$$

$$S_{14}=S_{23}=S_{24}=S_{13} \tag{A·8}$$

$$\begin{aligned}S_{33}=&j\omega\mu\frac{16R_a^2}{W_2^2}\int_{-\frac{\theta_0}{2}}^{\frac{\theta_0}{2}}d\varphi\int_{-\frac{\theta_0}{2}}^{\frac{\theta_0}{2}}d\varphi'\int_{|\alpha\varphi|}^{-|\alpha\varphi|+H+2W_1}dz\\&\cdot\int_{|\alpha\varphi'|}^{-|\alpha\varphi'|+H+2W_1}dz' G_{zz}(R_a,\varphi,z,R_a,\varphi',z')\\=&\frac{\omega\mu R_a^2}{4\pi W_2^2}\sum_{n=0}^{\infty}\sum_{m=1}^{\infty}(2-\delta_0)\left[\frac{\lambda^2J_n^2(\lambda R_a)}{k^2I_\lambda k_\lambda}I_{33}(k_\lambda)\right.\\&\left.-\frac{2jJ_n^2(\lambda R_a)}{k^2I_\lambda}I_{33\delta}\right]\end{aligned} \tag{A·9}$$

$$\begin{aligned}I_{33}(\xi)=&\frac{32}{j\xi n^2}\left[H\sin^2(\gamma)-\frac{d}{2}\sin 2\gamma\right.\\&+W_1-\frac{\frac{d}{2}\sin 2\gamma+W_1}{1-d^2\xi^2}\\&+\frac{1}{j\xi(1-d^2\xi^2)^2}(-\Lambda^+(\gamma)\Lambda^-(\gamma)-d^2\xi^2\end{aligned}$$

$$+2jd\xi\Lambda^{+}(\gamma)e^{-j\xi W_1}+\Lambda^{-2}(\gamma)e^{-j\xi H}-2jd\xi\Lambda^{-}(\gamma)e^{-j\xi(H+W_1)}-d^2\xi^2e^{-j\xi(H+2W_1)})\Big] \quad (A\cdot10)$$

$$I_{33\delta}=\frac{16}{n^2}\left(H\sin^2(\gamma)-\frac{d}{2}\sin(2\gamma)+W_1\right) \quad (A\cdot11)$$

$$S_{34}=j\omega\mu\frac{16R_a^2}{W_2^2}\int_{-\frac{\theta_0}{2}}^{\frac{\theta_0}{2}}d\varphi\int_{-\frac{\theta_0}{2}}^{\frac{\theta_0}{2}}d\varphi'\int_{|\alpha\varphi|}^{-|\alpha\varphi|+H+2W_1}dz\cdot\int_{|\alpha\varphi'|}^{-|\alpha\varphi'|+H+2W_1}dz'G_{zz}(R_a,\varphi,z,R_a,\pi+\varphi',z')$$

$$=\frac{\omega\mu R_a^2}{4\pi W_2^2}\sum_{n=0}^{\infty}\sum_{m=1}^{\infty}(2-\delta_0)\left[\frac{\lambda^2J_n^2(\lambda R_a)}{k^2I_\lambda k_\lambda}I_{34}(k_\lambda)-\frac{2jJ_n^2(\lambda R_a)}{k^2I_\lambda}I_{34\delta}\right] \quad (A\cdot12)$$

$$I_{34}(\xi)=-(-1)^nI_{33}(\xi) \quad (A\cdot13)$$

$$I_{34\delta}=-(-1)^nI_{33\delta} \quad (A\cdot14)$$

Finally the expression of $Z_{11}$ can be obtained by taking the summation of $S_{ij}$ as

$$Z_{11}=\sum_{i=1}^{4}\sum_{j=1}^{4}S_{ij}=\frac{\omega\mu R_a^2}{4\pi W_2^2}\sum_{p=0}^{\infty}\sum_{m=1}^{\infty}128\varepsilon_n\left[\frac{R_a^2J_n^2(\mu R_a)}{n^4I_\mu k_\mu}I(k_\mu)+\frac{J_n^2(\lambda R_a)}{n^2I_\lambda k_\lambda^3}\left(\frac{k^2}{\lambda^2}I(k_\lambda)+I_\delta(k_\lambda)\right)\right] \quad (A\cdot15)$$

where $n=2p+1$ and the function $I(\xi)$ and $I_\delta(\lambda)$ are given by

$$I(\xi)=\frac{1}{1-d^2\xi^2}\Big[j\xi\left(\frac{d}{2}\sin(2\gamma)+W_1\right)+\frac{\Lambda^{+}(\gamma)\Lambda^{-}(\gamma)+d^2\xi^2}{1-d^2\xi^2}-\frac{1}{1-d^2\xi^2}(2j\xi\Lambda^{+}(\gamma)e^{-j\xi W_1}+\Lambda^{-2}(\gamma)e^{-j\xi H}-2jd\xi\Lambda^{-}(\gamma)e^{-j\xi(H+W_1)}-d^2\xi^2e^{-j\xi(H+2W_1)})\Big] \quad (A\cdot16)$$

$$I_\delta(\xi)=-j\xi\left(H\sin^2(\gamma)-\frac{d}{2}\cos(2\gamma)+W_1\right) \quad (A\cdot17)$$

In Eqs. (A·2)-(A·17), the following notation is used,

$$\theta=W_2/R_a \qquad \alpha=2W_1/\theta$$

$$d=\alpha/n \qquad \gamma=n\theta_0/2$$

$$\Lambda^{\pm}(\gamma)=\sin\gamma\mp jd\xi\cos\gamma \qquad \dot{J}(x)=\frac{\partial J(x)}{\partial x}$$

where $\lambda$, $\mu$, $k_\lambda$, $k_\mu$, $I_\lambda$ and $I_\mu$ are defined by follows.

$$k_\mu=(k^2-\mu^2)^{\frac{1}{2}} \qquad k_\lambda=(k^2-\lambda^2)^{\frac{1}{2}}$$

$$I_\mu=\frac{a^2}{2\mu^2}\left(\mu^2-\frac{n^2}{a^2}\right)J_n^2(q_{nm})$$

$$I_\lambda=\frac{a^2}{2}\left(\frac{\partial J_n(x)}{\partial x}\Big|_{x=p_{nm}}\right)^2 \qquad \mu=\frac{q_{nm}}{a} \qquad \lambda=\frac{p_{nm}}{a}$$

and $p_{nm}$ and $q_{nm}$ are the roots of equations $J_n(p_{nm})=0$ and $\partial J_n(x)/\partial x|_{x=q_{nm}}=0$, respectively.

Equation (A·15) involves two terms, i.e, a term concerned with $I(k_\mu)$ and the other with $I(k_\lambda)$ and $I_\delta(k_\lambda)$. They decrease almost proportional to the order of $n^{-4}k_\mu^{-2}$ and $n^{-2}k_\lambda^{-2}\lambda^{-2}$ respectively, when $m$ or $n$ increases. Because $k_\lambda$, $k_\mu$ and $\lambda$ increase almost linearly with $m$ and $n$ when $m$ and $n$ are large enough, the double series summation converges rapidly.

**Qiang Chen** was born in Xi'an, China, on February 12, 1965. He received the B.E. degree from Xidian University, Xi'an, China, in 1986 and the M.E. degree from Tohoku University, Sendai, Japan, in 1991. He is now studying for the D.E. degree in the Department of Electrical Engineering, at the Tohoku University. He is currently involved in the research of RF antenna for MRI system.

**Kunio Sawaya** was born in Sendai, Japan, on February 21, 1949. He received the B.E., M.E., and D.E. degrees from Tohoku University, Sendai, Japan, in 1971, 1973, and 1976, respectively. He is presently an Associate Professor in the Department of Electrical Engineering at the Tohoku University. His areas of interests are antennas in a plasma, antennas for mobile communications, theory of diffraction, array antennas, antennas for plasma heating, and high-Tc superconducting antennas. He received the Young Scientists Award in 1981 and the Paper Award in 1988 both from the Institute of Electronics, Information and Communication Engineers of Japan. Dr. Sawaya is a member of the Institute of Electrical and Electronics Engineers and the Institute of Television Engineers of Japan.

**Saburo Adachi** was born on September 2, 1930 in Japan. He received the B.S., M.S., and Ph.D degrees in Electrical Engineering, all from the Tohoku University, Sendai, Japan in 1953, 1955 and 1958, respectively. From 1958 to 1960 he was on leave from the Tohoku University to join the Antenna Laboratory, the Ohio State University, Columbus, Ohio as a Research Associate and a Fullbright Scholar. He was an Associate Professor of Tohoku University from 1961 through 1970. He is presently a Professor in the Department of Electrical Engineering of the same University. He is also a Guest Research fellow of Communication Research Laboratory, Ministry of Posts and Telecommunications. His areas of interests are acattering and diffraction, antennas, radiation, and propagation in plasma, antennas for plasma heating, superconducting antennas, interaction between human body and electromagnetic wave, inverse scattering problems, antenna systems for mobile communications, etc. He received the Paper Awards, Publication Award, Achievement Award from the Institute of Electronics, Information and Communication Engineers of Japan. Dr. Adachi was elected Fellow of the IEEE on January 1, 1984 for his contributions to the theory and practice of antennas in plasma. He is currently President of Japanese URSI Committee, Vice President of the IEICE, and a member of the Engineering Academy of Japan.

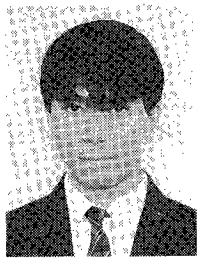

**Hisaaki Ochi** graduated in 1987 from the Dept. Control Eng., Fac. Eng. Sci., Osaka Univ., where he obtained a master's degree in Control Eng. in 1989 and affiliated with Hitachi, Ltd. He is engaged at Central Res. Lab. in research and development of MRI.

**Etsuji Yamamoto** obtained a Dr. of Eng. degree in 1987 from Hokkaido Univ. and then affiliated with Hitachi, Ltd. He is engaged in research on Magnetic Resonance Imaging (MRI) systems. Presently, he is Senior Researcher, Medical Electronics Research Center, Central Res. Lab. Hitachi, Ltd. He is a member of the Japan Society of Magnetic Resonance in Medicine, and the Japan Society of Medical Electronics and Biological Engineering.